The structural basis of integrin-linked kinase–PINCH interactions

Brian P. Chiswell, Rong Zhang, James W. Murphy, Titus J. Boggon[1], and David A. Calderwood[1]

Department of Pharmacology, Yale Cancer Center and Interdepartmental Program in Vascular Biology and Transplantation, Yale University School of Medicine, 333 Cedar Street, New Haven, CT 06520

Communicated by Joseph Schlessinger, Yale University School of Medicine, New Haven, CT, November 11, 2008 (received for review September 4, 2008)

The heterotrimeric complex between integrin-linked kinase (ILK), PINCH, and parvin is an essential signaling platform, serving as a convergence point for integrin and growth-factor signaling and regulating cell adhesion, spreading, and migration. We report a 1.6-Å crystal structure of the ILK ankyrin repeat domain bound to the PINCH1 LIM1 domain, revealing the molecular basis of ILK-PINCH interactions and providing a structural description of this region of ILK. This structure identifies 5 ankyrin repeats in ILK, explains previous deletion mutagenesis data, permits identification of ILK and PINCH1 point mutations that disrupt the interaction, shows how zincs are coordinated by PINCH1 LIM1, and suggests that conformational flexibility and twisting between the 2 zinc fingers within the LIM1 domain may be important for ILK binding. These data provide an atomic-resolution description of a key interaction in the ILK–PINCH–parvin scaffolding complex.

ankyrin repeat domain | LIM domain | IPP complex

The dynamic, spatially and temporally regulated assembly and disassembly of multiprotein complexes linking transmembrane integrin adhesion receptors to the actin cytoskeleton and intracellular signaling cascades is essential for the viability of multicellular animals. The integrin-linked kinase (ILK) was identified as an integrin β1 tail-binding protein (1) and localizes to sites of integrin-mediated cell adhesion in vitro and in vivo (2–4). Genetic analyses show that ILK and its binding partners play key roles in linking integrins to actin, and cell biological and biochemical studies support the view that ILK-containing complexes act as signaling platforms that are likely to be points of convergence of growth factor- and integrin-mediated signaling pathways (2–4). Here, we provide a structural description of ILK and show the molecular basis for its interaction with PINCH; an association critical to integrin-mediated cell adhesion, migration, spreading, and signaling.

Sequence analysis of ILK predicts an N-terminal ankyrin (ANK) repeat domain and a C-terminal protein kinase domain (Fig. 1*A*). Although catalytic activity of the ILK kinase domain remains controversial (2, 3), it is well accepted that ILK plays essential roles as an adaptor protein. Many of the downstream effects of integrins require the formation of a heterotrimeric complex between ILK, PINCH, and parvin (5, 6). This IPP complex (2) serves as a hub in integrin–actin and integrin-signaling networks (4), and in mammalian systems IPP complex formation precedes and is required for its correct targeting to adhesions (7). In addition, IPP complex formation protects its components from proteasomal degradation (8, 9).

As observed for ILK, PINCH is essential for normal integrin-mediated cell adhesion (2, 9, 10). There are 2 PINCH genes in mammals encoding closely related proteins, PINCH1 and PINCH2. PINCH1 is widely expressed throughout development, and PINCH1$^{-/-}$ mice die at the periimplantation stage, somewhat later than ILK or β1 integrin mutants, with defects in cell–matrix adhesions, cell polarity, and cell survival (10). PINCH2 has a more restricted expression, and, possibly because of compensation by up-regulated PINCH1, PINCH2$^{-/-}$ mice exhibit no overt phenotype (9). The domain structure of all PINCH family members consists of 5 LIM domains (Fig. 1*A*). LIM domains are composed of 2 zinc fingers and have been shown to be important for multiple protein–protein interactions (11). Solution structures for 4 isolated PINCH LIM domains have been determined, [LIM1 (1G47) (12), LIM2 (2D8X), LIM3 (2COR), and LIM4 (1NYP and 1U5S) (13, 14)], but no crystal structures are available. The ILK–PINCH interaction is mediated by ILK ANK repeat domain binding to PINCH LIM1 (5, 9, 12). This interaction is sufficient to protect ILK and PINCH from degradation and is required for correct IPP targeting to adhesions and regulation of cell spreading and migration (2, 9, 15).

Despite the critical importance of ILK-PINCH interactions in cytoskeletal organization and adhesion signaling the structural basis for their interaction has not previously been described. Here, we report the crystal structure of the ILK ANK repeat domain bound to PINCH1 LIM1 domain. This high-resolution structure reveals the molecular basis for the interaction between PINCH and ILK and provides a structural description of this region of ILK.

Results and Discussion

Overall Structure. To investigate the ILK–PINCH1 complex, the N-terminal 192 aa of human ILK, containing the predicted ANK repeats, and the LIM1 domain of human PINCH1 (amino acids 6–68) were expressed separately in *Escherichia coli*. Cells were mixed before lysis, and the ILK–PINCH1 complex was purified by tandem affinity tag purification, first by using the His tag on PINCH1 LIM1 and then the GST tag on ILK$^{1\text{-}192}$. Thrombin digestion removed both tags and C-terminal clipping produced a fragment spanning ILK$^{1\text{-}174}$. The ILK$^{1\text{-}174}$/PINCH1$^{6\text{-}68}$ complex remained intact through further rounds of ion-exchange and size-exclusion chromatography. The crystal structure of the complex was determined at 1.6-Å resolution (Fig. 1, supporting information (SI) Table S1 and Fig. S1). The final model includes residues 2–170 of ILK and 6–68 of PINCH1 fused to 9 N-terminal vector-derived residues (Fig. 1*B*). The structure shows a stoichiometric interaction between the 2 proteins and reveals that ILK contains 5 ANK repeats and that ANK repeats 2–5 all mediate an interaction with the PINCH1 LIM1 domain. The crystallized PINCH1 LIM1 domain is conformationally distinct from the previously solved NMR structure of PINCH1 LIM1 (12), with an intersubdomain twist of ≈65° occurring upon binding to ILK. The crystal structure reveals the molecular basis of the ILK–PINCH interaction.

Structure of the ANK Repeat Domain of ILK. The N-terminal domain of ILK contains 5 ANK repeats, the first of which was not evident

Author contributions: B.P.C., T.J.B., and D.A.C. designed research; B.P.C., R.Z., J.W.M., and T.J.B. performed research; B.P.C., T.J.B., and D.A.C. analyzed data; and T.J.B. and D.A.C. wrote the paper.

The authors declare no conflict of interest.

Data deposition: The coordinates and structure factors have been deposited in the Protein Data Bank, www.pdb.org (PDB ID code 3F6Q).

[1]To whom correspondence may be addressed. E-mail: david.calderwood@yale.edu or titus.boggon@yale.edu.

This article contains supporting information online at www.pnas.org/cgi/content/full/0811415106/DCSupplemental.

© 2008 by The National Academy of Sciences of the USA

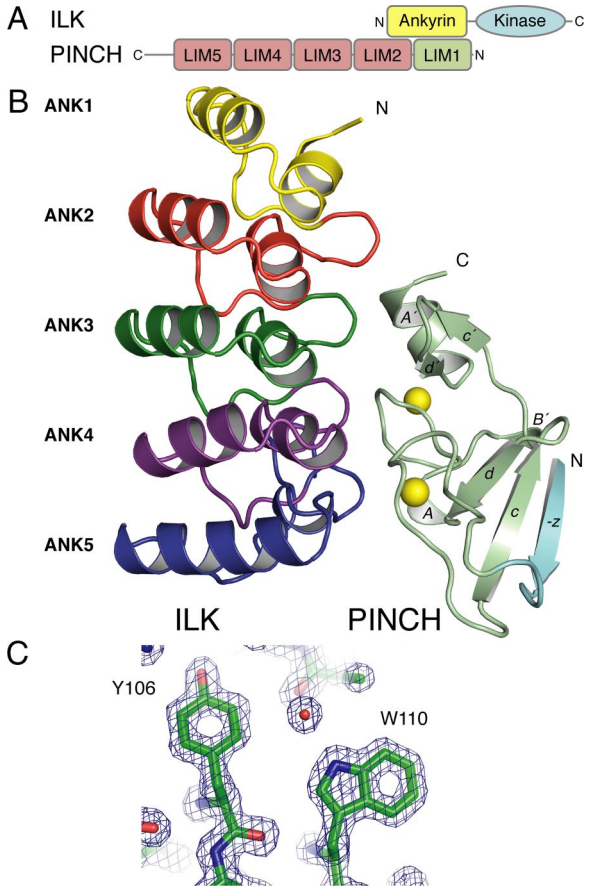

Fig. 1. Structure of the ILK ANK repeat domain in complex with PINCH LIM1. (*A*) Schematic showing the domains of ILK and PINCH. (*B*) Cartoon of the structure of the LIM1 domain of PINCH1 in complex with ILK. PINCH1 is shown in light green with zincs as yellow spheres and the vector-derived N-terminal β-strand (strand $-z$) in light blue. ILK is colored according to ANK repeat (ANK1 yellow; ANK2 red; ANK3 green; ANK4 purple; ANK5 blue). This color scheme is maintained throughout the manuscript. (*C*) Example $2F_o$-F_c electron density maps contoured at 1.5 σ. Clear density for ILK residues Tyr-106 and Trp-110 is visible. All figures are made by using PYMOL (www.pymol.org).

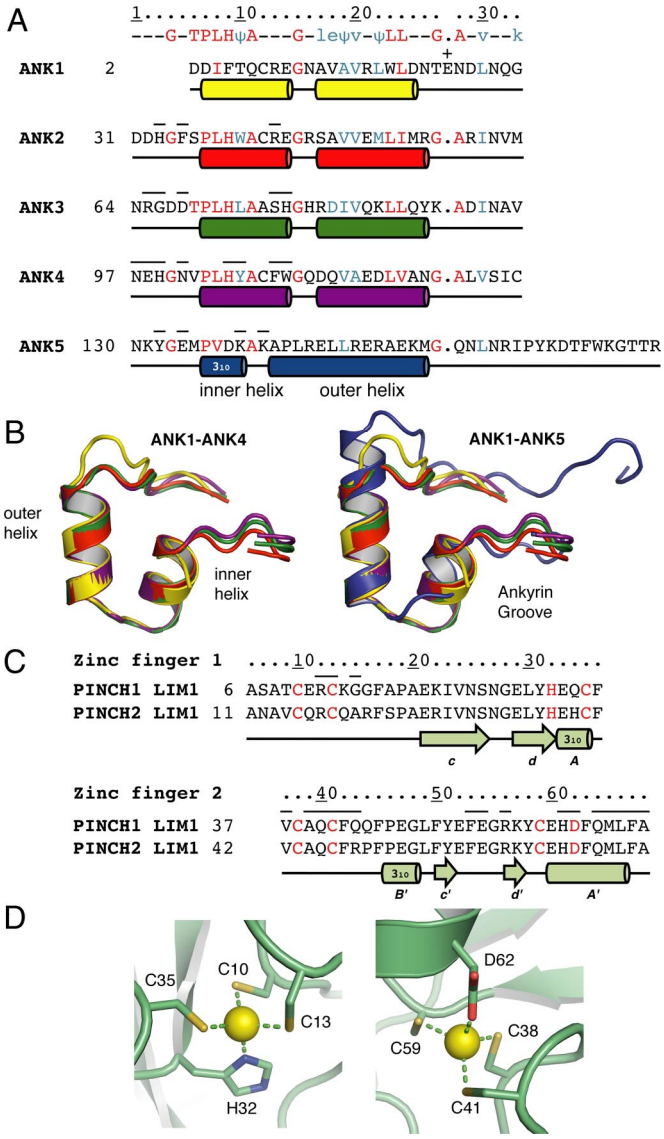

Fig. 2. Details of the ILK–PINCH1 structure. (*A*) Alignment of the ILK ANK repeats. The consensus ANK repeat sequence is shown on top, and the 33 residues are aligned in the harpin–helix–turn–helix style proposed in ref. 16. Highly conserved residues are colored red and capitalized, reasonably conserved residues are colored cyan and not capitalized. ψ Indicates a hydrophobic residue. ILK residues that conform to the consensus are the same color as the consensus residue. Residues that interact with PINCH are indicated by a bar. ANK1 does not include the loop residues and has an insertion at position 28, Glu^{24}, indicated by a "+." The inner helix of ANK5 is a 3_{10} helix, an unusual feature in ANK repeats. (*B*) Superposition of ILK ANK repeats. (*Left*) Superposition of ANK1 through ANK4. Insertion of Glu^{24} in ANK1 results in a bulge. (*Right*) Superposition of all of the ILK ANK repeats. ANK5 is divergent from ANK1–4, its inner helix has 3_{10} morphology that seems stabilized by a well-conserved salt bridge between Asp^{138} and Arg^{149}, and its outer helix concludes with an extra turn. (*C*) Alignment of PINCH1 LIM1 (GenBank Accession no. P48059) domain with PINCH2 LIM1 (GenBank Accession no. Q7Z4I7) domain. The extent of the N- and C-terminal zinc fingers (zinc fingers 1 and 2, respectively) are shown. Secondary structure features found in the crystal structure are indicated and labeled according to Grishin (18); neither zinc finger contains β-strands *a* or *b*. Zinc coordinating residues are colored red. Residues that interact with ILK are indicated by a bar. (*D*) Zinc-binding sites in PINCH1. N-terminal CCHC motif site (*Left*). C-terminal CCCD motif site (*Right*). Zinc-binding bond distances and angles are shown in Table S2.

in the original sequence-based assignment of 4 ANK repeats (ANK2–ANK5) (1). The consensus ANK repeat motif is a 33-aa repeat that folds into a hairpin–helix–turn–helix structure (Fig. 2*A*) (16). Two antiparallel α-helices from each repeat pack against one another, and the β-hairpin that links each pair of helices is oriented perpendicular to the helices to form a characteristic cross-sectional "L" shape. Within ANK repeat domains, adjacent repeats stack on top of one another such that the helices form helical bundles. The stacked repeats form a curved left-handed superhelical spiral (17). The interior surface of the spiral is concave and forms the "ankyrin groove," a feature that has been likened to a cupped hand, with the helices as the palm and the β-hairpins as fingers (16). This concave surface provides an ideal recognition site for intermolecular interactions (16, 17) and is the location of ILK interaction with PINCH.

In ILK, each ANK repeat contains 2 antiparallel helices that pack against one another and are separated by a short loop. In ANK repeats 2–5 (ANK2–ANK5), the first helix is preceded by a characteristic hairpin loop, termed the "finger" loop, the first repeat, ANK1, does not include this hairpin loop. In the classical description of ANK repeat proteins, this loop forms the β-hairpin of the hairpin–helix–turn–helix structure; however, not all ANK repeat proteins display the β-hairpin hydrogen-bonding pattern (17). In ILK, the β-hairpin hydrogen-bonding pattern is lacking, and the loops form type I β-turns.

The ILK ANK repeat domain is most similar to designed ANK repeat structures (*SI Text*). Comparison of the ANK repeats of ILK shows that there is good alignment between repeats ANK1 to

ANK4 with RMSD <1.1 Å for Cα atoms (*SI Text*). ANK1 contains a 1-residue insertion C-terminal to the outer helix (Fig. 2*A*). This insertion of a well-conserved surface exposed glutamic acid, Glu^{24}, results in a bulge of the ANK1 repeat (Fig. 2*B*). ANK5 is more divergent from ANK1–ANK4; the inner helix is a 3_{10} rather than an α-helix and the outer helix is 1 turn longer than those usually observed in ANK repeats (*SI Text*).

Structure of the LIM1 Domain of PINCH1. LIM domains are ≈55-aa tandem zinc finger domains containing 2 type VII treble clef zinc fingers (nomenclature *abcdA*) (11, 18) connected by a 2-residue flexible linker, with a consensus sequence of $CX_2CX_{16-23}HX_2CX_2CX_2CX_{16-21}CX_2(C/H/D)$ (11). The architecture of the LIM1 domain of PINCH1 is broadly similar to previously solved LIM domains but varies somewhat from that of canonical treble clef motifs. Briefly, these differences include the lack of the treble clef β-sheet *ab*, 3_{10}-helix propensity for the N-terminal zinc finger subdomain and a short 3_{10} helix formed by residues Pro^{46}–Gly^{48} (Fig. 2*C*; discussed in detail in *SI Text*). The 2 PINCH1 LIM1 zinc fingers overlay on one another with an RMSD of 1.7 Å over 27 residues [using secondary structure matching (19); Fig. S2].

Zinc seems to stabilize the fold of treble clef-type zinc fingers, reducing the need for a large hydrophobic core (18). In PINCH1 LIM1, the residues that ligate the 2 approximately tetrahedrally coordinated zincs are Cys^{10}, Cys^{13}, His^{32}, and Cys^{35} of the N-terminal subdomain and Cys^{38}, Cys^{41}, Cys^{59}, and Asp^{62} of the C-terminal subdomain (Fig. 2*D*; Table S2). These interactions form CCHC and CCCD zinc-binding modules. In contrast to the published solution structure of free PINCH1 LIM1 (12) but similar to the crystallographic studies for LMO4 (20), the C-terminal subdomain binds zinc with a CCCD module, not a CCCH module (Fig. S1). His^{61} of the previously described CCCH module is extended away from the zinc-binding site and forms a salt bridge with Glu^{98} of the ILK ANK4 repeat. We cannot exclude the possibility that the altered zinc coordination is due to ILK binding but favor the interpretation that the second zinc finger of PINCH1 LIM1 normally binds via a CCCD module.

Interaction Between ILK and PINCH. PINCH1 LIM1 is cradled in the highly conserved concave ANK groove of ILK and nestles between the fingers and palm of the ANK repeat structure (Figs. 3*D* and 4). The zinc-binding sites of PINCH1 LIM1 are on the same face and approximate to the ILK-binding site. For ILK, binding is mediated by ANK repeats 2–5, with ANK4 providing the most significant contributions. For PINCH1 LIM1, both zinc fingers interact with ILK. However, consistent with previous deletion mutagenesis and NMR analyses (12, 21), the C-terminal zinc finger is the primary mediator of the interaction. The interaction buries 895 $Å^2$ in ILK and 998 $Å^2$ in PINCH1 to give an average interface surface area of 947 $Å^2$. A total of 20 residues from ILK and 19 from PINCH1 LIM1 directly interact, forming 13 intermolecular H bonds and 148 intermolecular nonbonded contacts to make an interface with both hydrophobic and polar interactions (22) (Fig. 3).

Interface between each ILK ANK repeat and PINCH LIM1. The interaction between ILK and PINCH1 LIM1 can be analyzed by assessing the role of each ANK repeat individually. ANK2 constitutes the most N-terminal region of the PINCH1 LIM1-binding site in ILK. Two residues, Arg^{43} and His^{33}, form electrostatic interactions with the C-terminal zinc finger of PINCH1. Arg^{43} forms a salt bridge to Glu^{54}, which falls between strands *c′* and *d′* of the second PINCH1 zinc finger, and His^{33} hydrogen-bonds to the carbonyl oxygen of Met^{65} and the carboxyl terminal of PINCH1 LIM1. Phe^{35} is in nonbonding contact with Leu^{66} of PINCH1 (Figs. 4 and 5).

ANK3 contributes 5 residues to the interaction with PINCH1. Arg^{65}, Gly^{66}, and Asp^{68} are ANK3 finger residues, and Ser^{76} and His^{77} are palm residues. Arg^{65} forms an H bond with the carbonyl oxygen of PINCH1 Gln^{64}, and Gly^{66} is in nonbonding contact with Leu^{66} of PINCH1. Gln^{64} and Leu^{66} fall within the second turn of helix *A′* for the C-terminal PINCH1 zinc finger (Figs. 4 and 5). Previous mutagenesis of PINCH1 Gln^{40} has shown this residue to be integral to the PINCH–ILK interaction (7). The crystal structure now reveals that this is probably due to the formation of an H bond between the side chains of Gln^{40}, which lies in the zinc knuckle of the second zinc finger, and ILK Asp^{68}. His^{77} and Ser^{76} are the terminating residues of the ANK2 inner helix, and both interact with Arg^{56} of PINCH1. Although Arg^{56}, a residue that falls between strands *c* and *d* of the second PINCH1 zinc finger, H-bonds to both the backbone carbonyl and the side-chain hydroxyl oxygens of Ser^{76}; it is also sandwiched between His^{77} and Trp^{110} of ANK4 to form a π–cation–π stack (Figs. 4 and 5).

ANK4 is the repeat most intrinsic to the ILK–PINCH1 interaction (Figs. 4 and 5). Four residues from the ANK4 inner helix (Trp^{110}, Phe^{109}, Tyr^{106}, and His^{105}) and 4 residues from the ANK4 hairpin (Asn^{97}, Glu^{98}, His^{99}, and Asn^{101}) contribute to the interaction. A hydrophobic core to the ILK–PINCH1 interaction

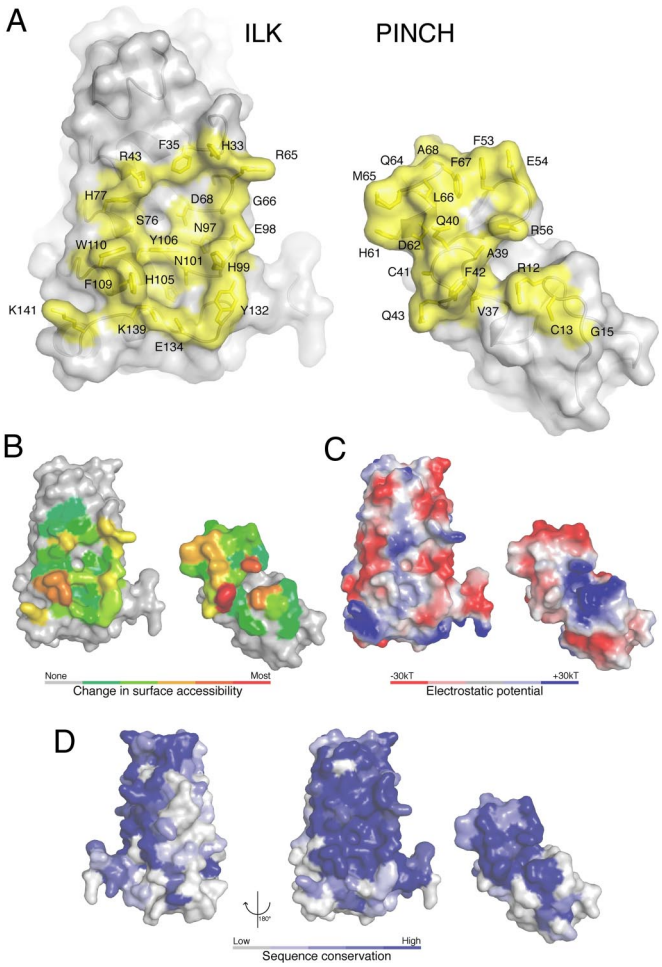

Fig. 3. Surfaces of ILK and PINCH1. An open-book format is used, with ILK on the left and PINCH1 on the right. (*A*) Interacting residues. Surfaces colored yellow for residues that interact and gray for residues that do not interact between ILK and PINCH1. (*B*) Surface accessibility. Colored according to absolute difference in surface accessibility (NACCESS, S. Hubbard and J. Thornton, www.bioinf.manchester.ac.uk/naccess/). Residues with no change in surface accessibility are colored gray, small changes are in green and larger changes in surface accessibility on complex formation are yellow through red. This clearly shows the importance of PINCH1 residue, Phe^{42}, to the interaction. (*C*) Electrostatic potential representation (+30 kT, blue; −30 kT, red). (*D*) Sequence conservation. Surface colored by sequence conservation based on alignment of 19 PINCH LIM1 sequences and 28 ILK sequences (29). Darker blue indicates higher conservation. The leftmost image shows the reverse face of ILK.

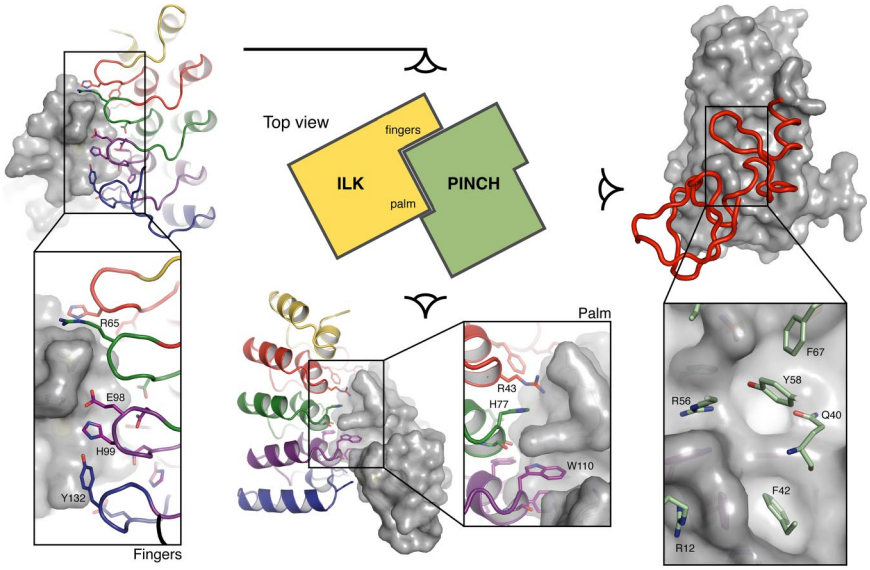

Fig. 4. Architecture of the interaction. (*Center*) Illustration of a top-view schematic of the ILK interaction with PINCH1. Three views show this interaction from different angles. (*Left*) Toward PINCH1 (gray surface) from the ILK ANK repeat finger side of the interaction. Lower images are toward PINCH1 (gray surface) from the ILK ANK repeat palm side of the interaction. (*Right*) Toward ILK (gray surface). Shown in red is PINCH1 backbone trace. Blown-up views show labels for residues involved in the interaction.

is formed by the insertion of the C-terminal PINCH1 zinc knuckle residue, Phe^{42}, into a pocket made by Phe^{109}, Tyr^{106}, His^{105}, Asn^{101}, and Lys^{139} of ANK5. This hydrophobic core seems critical to formation of an ILK–PINCH1 complex. In addition to bounding this hydrophobic pocket, Phe^{109} forms a π-cation interaction with the guanidinium group of Arg^{12}, and Arg^{12} forms a bidentate H bond to its carbonyl oxygen. Arg^{12} is a component of the N-terminal PINCH1 zinc knuckle. In addition to bounding the Phe^{42} hydrophobic pocket, ANK4 residues, Tyr^{106} and Asn^{101}, both form H bonds to the backbone carbonyl oxygen of PINCH1 Gln^{40}. In the ANK4 hairpin there are 4 residues that interact with PINCH1. Asn^{101} has been discussed above, Asn^{97} H-bonds to Asp^{68} of ANK3 and is in nonbonding contact with Gln^{40} of PINCH1. The Asn^{97}–Asp^{68} interaction seems to stabilize the orientation of Asp^{68} for H-bonding to Gln^{40} of PINCH1. The 2 remaining hairpin residues, His^{99} and Glu^{98}, form salt bridges to residues of the first turn of helix A' in the C-terminal PINCH1 LIM1 zinc finger, His^{61} and Asp^{62}. Glu^{98} forms a salt bridge to His^{61}, and His^{99} forms a salt bridge to Asp^{62}. Asp^{62} is the zinc-coordinating Asp of the PINCH1 LIM1 CCCD motif.

ANK5, the C-terminal ANK repeat, contributes 4 residues to the ILK–PINCH1 interaction. ANK5 finger residues Tyr^{132} and Glu^{134} both interact with Gln^{43}, a residue that falls immediately subsequent to the second LIM1 zinc knuckle. Lys^{139} is part of the ANK5 3_{10} inner helix, forms part of the Phe^{42} hydrophobic pocket, and makes a salt bridge with Glu^{134} of ANK5. This salt bridge may help stabilize the 3_{10} helix of ANK5. Finally, Lys^{141} forms an H bond to the backbone carbonyl of Cys^{13}, a zinc-coordinating residue in the C-terminal PINCH1 zinc finger. Lys^{141} falls between the inner and outer ANK5 helices and is outside of the ILK ankyrin groove.

Role of ANK1. ANK1 does not interact directly with the LIM1 domain of PINCH1; however, mutagenesis data suggest that residues in ANK1 play a role in the interaction with PINCH (7). The location of the C terminus of the PINCH1 LIM1 domain in this crystal structure, combined with the conservation of ILK in this region (Fig. 3*D*), suggest that LIM2 may contribute to the ILK–PINCH interaction by packing against ANK1. Further studies are necessary to test this hypothesis.

PINCH perspective. There are 3 particularly striking features of the interaction from the perspective of PINCH. First, the seeming importance of Phe^{42} to the integrity of the PINCH–ILK interaction; second, the extended conformation of Arg^{12} and Arg^{56} to form cation–π and H-bond interactions with multiple ILK residues; and third, the seeming importance of the salt bridges formed between His^{61} and Asp^{62} of PINCH1 and Glu^{98} and His^{99} of ILK (Fig. 5). All of these residues, except Arg^{56}, are in close proximity to the zinc-binding sites, indeed, Asp^{62} is a zinc-coordinating residue, and His^{61} is directly proximal to the zinc-binding site and was previously thought to be a zinc-coordinating residue (12).

Mutagenesis studies. To investigate the functional role of significant residues in the ILK–PINCH1 interface and to understand the role of the N- and C-terminal zinc fingers of PINCH1 LIM1, we generated point mutations in the ILK ANK repeat and PINCH1 LIM1 domains and analyzed binding of the purified proteins. First, structural analysis of the ILK–PINCH1 complex shows that the largest surface area buried for an individual residue in the interface is for Phe^{42} of PINCH1 (Fig. 3*B*). Introduction of a F^{42}A point mutation resulted in a near complete loss of ILK binding (Fig. 5*C*), suggesting that Phe^{42} is central to the stability of the complex. The importance of the hydrophobic interaction between ILK and PINCH1 LIM1 is confirmed by a L^{66}D mutation, which also significantly reduces ILK binding. Second, an interesting feature of the interaction is the presence of 2 salt bridges formed between residues of the ANK4 hairpin and the helix A' of PINCH1. To investigate whether these ion pairs play significant roles in stabilization of the complex, we introduced both charge reversal and removal mutations. We mutated the salt bridges between ILK His^{99} and PINCH1 Asp^{62} and between Glu^{98} of ILK and His^{61} of PINCH1. Both charge reversal by ILK H^{99}D, a mutation that likely leads to repulsion of Asp^{62} in PINCH1, and charge removal by PINCH1 D^{62}A, a mutation that may result in both ablation of the salt bridge and altered zinc binding for the C-terminal zinc finger, reduce overall binding by $\approx$75% (Fig. 5*C*). Although charge removal of the second salt bridge between Glu^{98} of ILK and His^{61} of PINCH1 by mutation E^{98}A does not significantly alter the observed binding, charge reversal by the H^{61}D mutation results in $\approx$50% reduced binding. These salt bridges are proximal to the zinc-binding site for the C-terminal PINCH1 LIM1 zinc finger and

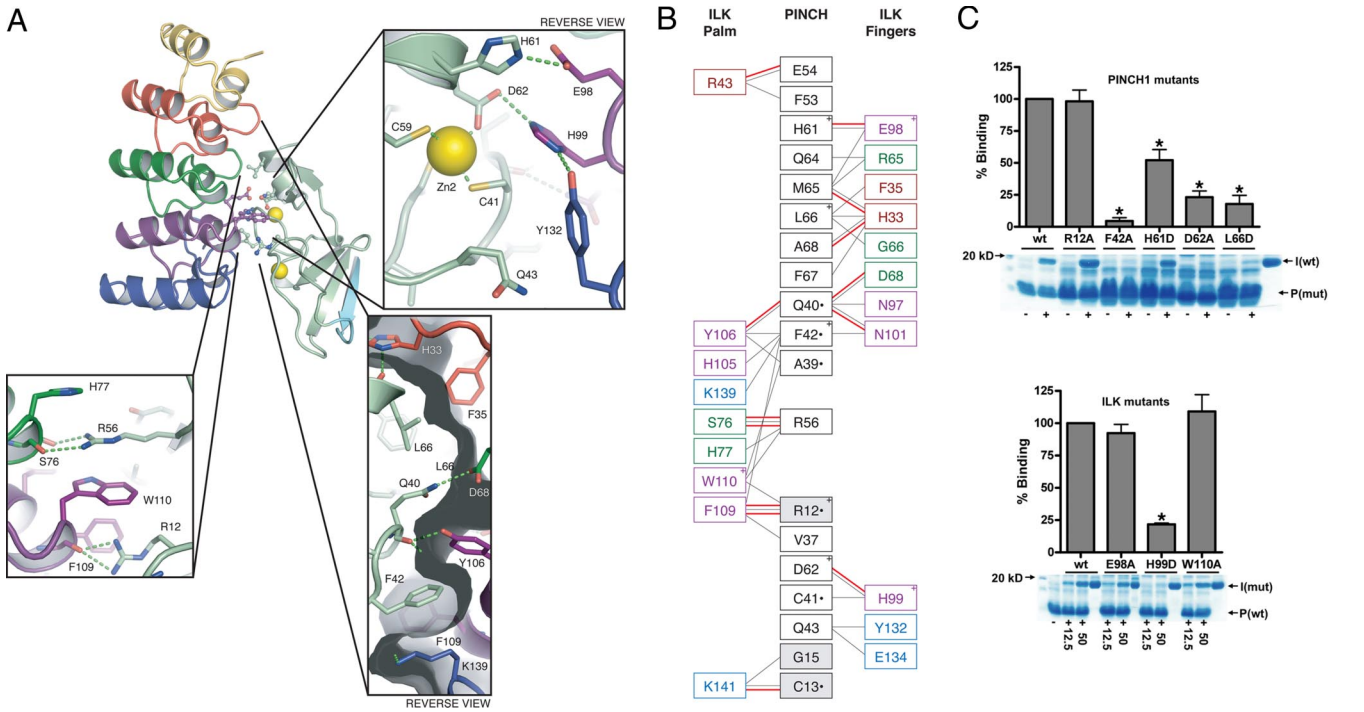

Fig. 5. Closeup of ILK–PINCH1 interaction. (*A*) Closeups of the important features of the interaction between ILK and PINCH1. The His^{99}–Asp^{62} and His^{61}–Glu^{98} salt bridges are shown in the top right pullout, and the extended Arg^{56} and Arg^{12} are seen in the bottom left pullout. The surface of ILK is shown in transparent gray in the lower right pullout to illustrate the hydrophobic surface that Phe^{42} and Leu^{66} interact with. H-bonds indicated with green dashed lines. Residues on which we performed mutagenesis studies are shown in ball-and-stick format in the central cartoon. (*B*) Map of the interactions between ILK and PINCH1. H bonds are shown as red lines and nonbonding contacts as black lines. ILK ''palm'' and ''finger'' residues are shown on 2 sides of PINCH1. ILK residues are colored according to ANK repeat: ANK2, red; ANK3, green; ANK4, purple; ANK5, blue. Residues from the N-terminal zinc finger of PINCH1 are shaded gray. PINCH1 residues that are part of a zinc knuckle or are zinc-coordinating are indicated with a ''●.'' Residues that were mutated are indicated with a ''+.'' (*C*) Mutagenesis of ILK–PINCH-binding interface. Pull-down assays were performed with PINCH1 LIM1-coated beads and thrombin-cleaved $ILK^{1\text{-}192}$ constructs. Bound protein was eluted in SDS under reducing conditions. Each lane represents a separate assay conducted in the presence (+) or absence (−) of ILK. For the PINCH mutants, 50 μg of wild-type ILK [I(wt)] was added to the PINCH-coated beads [P(mut)]; for the ILK mutants, either 12.5 or 50 μg of ILK [I(mut)] was added to the coated beads [P(wt)]. Binding in 50-μg assays was quantified by densitometry, normalized to bead-coating, and expressed as a percentage of wild-type (wt) binding in each experiment (mean ± SE, $n \geq 3$). *, $P < 0.01$ by paired *t* test.

suggest an important structural role for zinc in the interface between ILK and PINCH1. Finally, to investigate the importance of the interaction between the N-terminal zinc finger of LIM1 and ILK, we introduced point mutation $R^{12}A$. Arg^{12} is extended toward ILK ANK4; it H-bonds to the backbone carbonyl of Phe^{109}, and forms a cation–π stack with this residue. Loss of the ability to form these interactions does not deleteriously alter ILK–PINCH1 binding (Fig. 5*C*). These results confirm that the interaction between ILK and PINCH1 LIM1 is primarily mediated by the C-terminal zinc finger of PINCH1 LIM1.

Potential for PINCH2 binding to ILK. PINCH1 and PINCH2 share 85% sequence identity and both bind ILK (23). PINCH1 is more widely expressed than PINCH2, but both proteins have overlapping functions and can compete for binding to ILK, and PINCH2 expression can partially rescue some cellular phenotypes associated with loss of PINCH1 (8, 9, 23). Mapping the nonidentical residues to the surface of PINCH1 shows that only 2 residues that constitute part of the PINCH ILK-binding site differ between PINCH1 and PINCH2; the residues in the same position as Gly^{15} and Gln^{43} in PINCH1 are Ala and Arg in PINCH2 (Fig. S3). These differences occur on the periphery of the interface, suggesting that PINCH2 LIM1 and PINCH1 LIM1 bind ILK in a similar way.

Twisting of PINCH1 LIM1 upon Association with ILK. The individual LIM domain zinc fingers are structurally well conserved between the crystal and NMR structures; however, because of changes in the orientation of the zinc fingers with respect to one another, RMSD comparisons over the whole LIM domains show higher divergence (*SI Text*). In a number of published LIM domain NMR structures, the tandem zinc finger architecture of the LIM domain allows significant conformational flexibility (13, 24, 25). This rotation of LIM subdomains around an effective hinge in the linker can be large and can vary in solution (24), suggesting that the LIM architecture has evolved to easily alter the orientation of both subdomains to one another. The role of this flexibility has not been demonstrated. Analysis of the crystal structure of PINCH1 LIM1 in complex with ILK shows a significant ''twist'' when compared with the previously solved NMR structure of unbound PINCH1 LIM1 (12). Inspection of the difference between the NMR and crystal structures shows this twist between structures to be ≈65° [DYNDOM (26)]. This large movement results from an effective hinge axis around residues Phe^{36} and Val^{37} allowing the two zinc fingers to orient in relation to one another (Fig. S4) and may contribute to the ability of LIM1 to make intermolecular interactions.

Comparison of ILK–PINCH binding with Other Protein Complexes. ***ANK domain interactions.*** Previously described intermolecular interactions of ANK repeat proteins show that the primary mediator of these interactions is the concave surface situated between the fingers and palm of the ''ankyrin groove'' (16, 17). The interaction between ILK and PINCH provides a classic example of molecular utilization of this architecture—the interaction with PINCH is almost entirely mediated by a contiguous surface in the ankyrin groove.

LIM domain interactions. There are currently 3 crystal structures of LIM domains: the tandem LIM1 and LIM2 of LMO in complex

with Ldb1 (20, 27) and the crystal structure of LIM3 of TES in complex with Mena (28). The interaction between PINCH and ILK occurs on the zinc knuckle side of the PINCH LIM1 domain; this is a comparable intermolecular interface with that seen in TES for the TES–Mena complex (Fig. S5). The PINCH interface with ILK extends slightly more C-terminal on LIM1 than the TES–Mena interface does on TES, and the orientations of bound ILK and Mena are also slightly rotated compared with the LIM domain. The similarity of the PINCH–ILK interaction to that of TES with Mena is in sharp contrast to the interaction between LMO4 and Lbd1, an association that occurs on the opposite face of the LMO4 LIM domains and forms an extended β-zipper.

Potential PINCH intermolecular binding site. The crystal structure of PINCH in complex with ILK reveals a structural feature that may suggest a protein–protein interface for PINCH. The crystallized PINCH construct included 9 N-terminal residues, SENLYFQGS, which mediate one of the primary crystal lattice interactions and are likely to be critical to formation of the crystals (Fig. S6). Interestingly, the vector sequence also forms an antiparallel β-sheet (strand $-$z in Fig. 1*B*) with the *cd* β-sheet of the N-terminal LIM1 zinc finger. For LMO4 bound to Lbd1 (20), the N-terminal zinc fingers of both the LIM1 and LIM2 domains of LMO4 are critical to the β-zipper interface with Lbd1. Comparison of the crystal packing interaction found in the ILK-PINCH crystal with the LMO4-Lbd1 β-zipper interface reveals that the topologies of these interfaces are very similar (Fig. S7). Furthermore, the residues in PINCH that form a β-sheet with the vector sequence, Ile^{23} to Ser^{26}, are well conserved, and Val^{24}, Asn^{25}, and Ser^{26} are invariant in 19 PINCH LIM1 sequences analyzed. Therefore, we hypothesize that PINCH LIM1 may also form protein–protein interactions on its "reverse" side, distal to ILK. Further studies will be required to investigate this potential site of protein–protein interaction.

Summary

The IPP complex plays essential scaffolding roles transducing signals among integrins, growth factors, and the cytoskeleton, thus regulating cell morphology and behavior. The IPP complex is considered a promising target for cancer therapies, and genetic analyses confirm the importance of its components (2, 3). However, until now, relatively little was known about the structural basis of IPP complex formation. Our crystal structure of the ILK–PINCH complex provides an atomic-resolution description of part of the IPP complex, reveals the presence of 5 ANK repeats in ILK, explains previous deletion mutagenesis data, permits identification of point mutations in ILK and PINCH1 that disrupt the interaction, shows how zinc is coordinated by the PINCH1 LIM1 domain, and suggests that conformational flexibility of the LIM1 domain is likely to be important for binding to ligands. This provides key information for future analysis of the in vivo functions of the IPP complex.

Materials and Methods

Protein Complex Production and Purification. Recombinant GST-tagged human ILK^{1-192} and His-tagged $PINCH1^{6-68}$ were produced in *E. coli*, the complex was purified by tandem affinity tag purification, and the tags were removed with thrombin as described in *SI Text*. Mass spectrometry and N-terminal sequencing revealed internal thrombin proteolysis of ILK^{1-192} to generate a fragment spanning ILK^{1-174}. The cleaved complex was further purified by ion-exchange chromatography and concentrated to 13.5 mg/ml (*SI Text*).

Crystallography. Crystals grew in 20% PEG 3350, 0.2 M sodium formate, were cryoprotected in 35% PEG 3350, 0.2 M sodium formate, 0.5 M sodium iodide, and flash frozen in a stream of nitrogen vapor at 100 K. X-ray data were collected on the home source and the structure solved by molecular replacement (*SI Text*). Data collection and refinement statistics are shown in Table S1. Structure analyses were conducted primarily by using the CCP4 suite (19).

Binding Assays. $PINCH^{6-68}$ mutants were expressed as described for wild-type PINCH. Cells were lysed as described above, and the His-tagged PINCH constructs were bound to His-bind resin. PINCH-coated resin was washed with 50 mM sodium phosphate, 20 mM imidazole, and 300 mM NaCl (pH 8.0). ILK^{1-192} mutants were expressed and lysed as described above, purified on glutathione Sepharose beads, washed, and cleaved from the beads with thrombin. PINCH-coated resin was incubated with the cleaved ILK^{1-192} constructs in 500 mL of lysis buffer for 1 h at 23 °C with constant rocking. The resin was washed with 50 mM sodium phosphate, 5 mM imidazole, and 300 mM NaCl (pH 8.0). Bound protein was eluted with SDS/PAGE sample buffer containing 2-mercaptoethanol and analyzed by SDS/PAGE.

ACKNOWLEDGMENTS. We thank A. Kumar, K. Reinisch, A. Koleske, and B. Turk. Modified pET32 was designed by F. Poy. This work was supported by a Swebelius Cancer Research Award from the Yale Cancer Center. T.J.B. was an American Society of Hematology Scholar. B.P.C. was supported by Neuropharmacology (T32NS007136) and Vascular Research (T32HL007950) Postdoctoral Training Grants from the National Institutes of Health.

1. Hannigan GE, *et al.* (1996) Regulation of cell adhesion and anchorage-dependent growth by a new β1-integrin-linked protein kinase. *Nature* 379:91–96.
2. Legate KR, Montanez E, Kudlacek O, Fassler R (2006) ILK, PINCH and parvin: The tIPP of integrin signalling. *Nat Rev Mol Cell Biol* 7:20–31.
3. Hannigan G, Troussard AA, Dedhar S (2005) Integrin-linked kinase: A cancer therapeutic target unique among its ILK. *Nat Rev Cancer* 5:51–63.
4. Wu C (2005) PINCH, N(i)ck and the ILK: Network wiring at cell–matrix adhesions. *Trends Cell Biol* 15:460–466.
5. Tu Y, Li F, Goicoechea S, Wu C (1999) The LIM-only protein PINCH directly interacts with integrin-linked kinase and is recruited to integrin-rich sites in spreading cells. *Mol Cell Biol* 19:2425–2434.
6. Tu Y, Huang Y, Zhang Y, Hua Y, Wu C (2001) A new focal adhesion protein that interacts with integrin-linked kinase and regulates cell adhesion and spreading. *J Cell Biol* 153:585–598.
7. Zhang Y, *et al.* (2002) Assembly of the PINCH-ILK-CH-ILKBP complex precedes and is essential for localization of each component to cell–matrix adhesion sites. *J Cell Sci* 115:4777–4786.
8. Fukuda T, Chen K, Shi X, Wu C (2003) PINCH-1 is an obligate partner of integrin-linked kinase (ILK) functioning in cell shape modulation, motility, and survival. *J Biol Chem* 278:51324–51333.
9. Stanchi F, *et al.* (2005) Consequences of loss of PINCH2 expression in mice. *J Cell Sci* 118:5899–5910.
10. Li S, *et al.* (2005) PINCH1 regulates cell–matrix and cell–cell adhesions, cell polarity and cell survival during the peri-implantation stage. *J Cell Sci* 118:2913–2921.
11. Kadrmas JL, Beckerle MC (2004) The LIM domain: From the cytoskeleton to the nucleus. *Nat Rev Mol Cell Biol* 5:920–931.
12. Velyvis A, Yang Y, Wu C, Qin J (2001) Solution structure of the focal adhesion adaptor PINCH LIM1 domain and characterization of its interaction with the integrin-linked kinase ankyrin repeat domain. *J Biol Chem* 276:4932–4939.
13. Velyvis A, *et al.* (2003) Structural and functional insights into PINCH LIM4 domain-mediated integrin signaling. *Nat Struct Biol* 10:558–564.
14. Vaynberg J, *et al.* (2005) Structure of an ultraweak protein–protein complex and its crucial role in regulation of cell morphology and motility. *Mol Cell* 17:513–523.
15. Zhang Y, Guo L, Chen K, Wu C (2002) A critical role of the PINCH-integrin-linked kinase interaction in the regulation of cell shape change and migration. *J Biol Chem* 277:318–326.
16. Sedgwick SG, Smerdon SJ (1999) The ankyrin repeat: A diversity of interactions on a common structural framework. *Trends Biochem Sci* 24:311–316.
17. Mosavi LK, Cammett TJ, Desrosiers DC, Peng ZY (2004) The ankyrin repeat as molecular architecture for protein recognition. *Protein Sci* 13:1435–1448.
18. Grishin NV (2001) Treble clef finger—A functionally diverse zinc-binding structural motif. *Nucleic Acids Res* 29:1703–1714.
19. Collaborative Computational Project 4 (1994) The CCP4 suite: Programs for protein crystallography. *Acta Crystallogr D* 50:760–763.
20. Deane JE, *et al.* (2004) Tandem LIM domains provide synergistic binding in the LMO4:Ldb1 complex. *EMBO J* 23:3589–3598.
21. Li F, Zhang Y, Wu C (1999) Integrin-linked kinase is localized to cell–matrix focal adhesions but not cell–cell adhesion sites and the focal adhesion localization of integrin-linked kinase is regulated by the PINCH-binding ANK repeats. *J Cell Sci* 112:4589–4599.
22. Laskowski RA (2001) PDBsum: Summaries and analyses of PDB structures. *Nucleic Acids Res* 29:221–222.
23. Zhang Y, Chen K, Guo L, Wu C (2002) Characterization of PINCH-2, a new focal adhesion protein that regulates the PINCH-1-ILK interaction, cell spreading, and migration. *J Biol Chem* 277:38328–38338.
24. Kloiber K, Weiskirchen R, Krautler B, Bister K, Konrat R (1999) Mutational analysis and NMR spectroscopy of quail cysteine and glycine-rich protein CRP2 reveal an intrinsic segmental flexibility of LIM domains. *J Mol Biol* 292:893–908.
25. Deane JE, *et al.* (2003) Structural basis for the recognition of ldb1 by the N-terminal LIM domains of LMO2 and LMO4. *EMBO J* 22:2224–2233.
26. Lee RA, Razaz M, Hayward S (2003) The DynDom database of protein domain motions. *Bioinformatics* 19:1290–1291.
27. Jeffries CM, *et al.* (2006) Stabilization of a binary protein complex by intein-mediated cyclization. *Protein Sci* 15:2612–2618.
28. Boeda B, *et al.* (2007) Tes, a specific Mena interacting partner, breaks the rules for EVH1 binding. *Mol Cell* 28:1071–1082.
29. Landau M, *et al.* (2005) ConSurf 2005: The projection of evolutionary conservation scores of residues on protein structures. *Nucleic Acids Res* 33:W299–W302.